Computational and Theoretical Chemistry 991 (2012) 141–149

Contents lists available at SciVerse ScienceDirect

Computational and Theoretical Chemistry

journal homepage: www.elsevier.com/locate/comptc

Theoretical study of the mechanisms and rate constants on the reaction of H_2CNH with $O(^3P)$

Shida Gong, Chaoyang Wang *, Qianshu Li *

MOE Key Laboratory of Theoretical Chemistry of Environment, Center for Computational Quantum Chemistry, South China Normal University, Guangzhou 510006, PR China

ARTICLE INFO

Article history:
Received 31 December 2011
Received in revised form 11 April 2012
Accepted 11 April 2012
Available online 19 April 2012

Keywords:
Reaction mechanisms
H-abstraction
Rate constants

ABSTRACT

The multiple-pathway reaction system of H_2CNH and $O(^3P)$ has been investigated by ab initio methods. The optimized geometries and frequencies of all stationary points as well as the minimum energy paths (MEPs) are computed at the QCISD/cc-pVDZ level. The single point energies of the stationary points are refined at the QCISD(T)/aug-cc-pVTZ level. The rate constants of two H-abstraction pathways, $H_2CNH + O \rightarrow H_2CN + OH$ and $H_2CNH + O \rightarrow HCNH + OH$, are evaluated by conventional transition state theory (TST) and improved canonical variational transition state theory (ICVT) methods at the temperature range from 200 to 2500 K. Small-curvature tunneling (SCT) effect is taken into consideration. The computational results show that the variational effect for reaction $H_2CNH + O \rightarrow H_2CN + OH$ is larger than that for reaction $H_2CNH + O \rightarrow HCNH + OH$. In the lower temperature range, the SCT effect is important for the H-abstractions. Theoretical rate constants are generally close to experimental data. The ICVT/SCT theoretical rate constants are expressed in three-parameter formula as $k = 1.64 \times 10^{-17} T^{1.81} \exp(-962.61/T)$ cm^3 molecule^{-1} s^{-1} for the former pathway and $k = 2.98 \times 10^{-19} T^{2.43} \exp(-692.65/T)$ cm^3 molecule^{-1} s^{-1} for the latter pathway.

1. Introduction

The title reaction system is important to atmosphere and combustion reactions. Kantak et al. [1] and Williams and Fleming [2] discovered that the photochemical pollutant NO is contained in the fuel-nitrogen-HCN complexes which includes H_2CNH and O. Yang et al. claimed that the reaction of singlet H_2CNH and $O(^3P)$ is one reason for the consumption of ozone and one source of oxynitride in the air [3]. Tomeczek and Gradoń considered the reaction $H_2CNH + O \rightarrow H_2CN + OH$ is one possible step of a series reactions from the reactants $N_2O + CH_3$ to the products HCN + OH according to their experiments at constant temperature of 1800 K [4]. High reactivity makes $O(^3P)$ involved in a large quantities of atmospheric reactions with saturated or unsaturated hydrocarbons or their derivatives [5–9]. Among them hydrogen abstraction (H-abstraction) reaction is usual. The H-abstraction reaction product, OH radical, is an important partner in ozone depletion mechanism [10]. And $O(^3P)$ itself is also relevant to many atmospheric reactions related to ozone [6–9]. H_2CNH plays a significant role in many chemical reactions [11] and is also attractive for astrophysicists because it is thought to be an important prebiotic molecule and is supposed to form glycine [12]. H_2CNH is detected astronomically and its spectrum data are obtained [12–28]. Singlet and triplet H_2CNH are investigated experimentally and theoretically [29–40].

For the title reaction, the rate constants of two H-abstraction reaction pathways, $H_2CNH + O \rightarrow H_2CN + OH$ and $H_2CNH + O \rightarrow HCNH + OH$, were obtained experimentally by a few research groups. In studying the formation of HCN in flames via N_2O and NNH reacting with CH_i radicals at 1800 K, Tomeczek and Gradoń suggested a three-step mechanism as: $N_2O + CH_3 \rightarrow H_2CNH + NO$, $H_2CNH + O \rightarrow H_2CN + OH$, and $H_2CN + O \rightarrow HCN + OH$. But the second and the third steps were just proposed as probably steps and the reliable experimental measurements for the rate constants of them are not available. Thus a numerical modeling way has been chosen to adjust the rate constants of reaction $H_2CNH + O \rightarrow H_2CN + OH$, which is expressed as $k = 1.62 \times 10^{10} T^{1.25} \exp(-2405.58/T)$ cm^3 mol^{-1} s^{-1} [4]. Dean and Bozzelli listed the rate constants in their book [41] which are estimated to be $k = 1.7 \times 10^8 T^{1.5} \exp(-2330.04/T)$ cm^3 mol^{-1} s^{-1} for reaction $H_2CNH + O \rightarrow H_2CN + OH$ and $k = 2.2 \times 10^8 T^{1.5} \exp(-2719.55/T)$ cm^3 mol^{-1} s^{-1} for reaction $H_2CNH + O \rightarrow HCNH + OH$ by DHT (Direct Hydrogen Transfer) method. Kantak et al. estimated the above two rate constants at the temperature between 600 and 1400 K using the Senkan method [1], in which the rate constants are $k = 3.16 \times 10^8 T^{2.0} \exp(-3069.81/T)$ cm^3 mol^{-1} s^{-1} and $k = 3.16 \times 10^8 T^{2.0} \exp(-5032.48/T)$ cm^3 mol^{-1} s^{-1}, respectively. Polášek et al. prepared the simplest organic nitrone, CH_2=N(H)—O, transiently in the gas phase by femtosecond collisional

* Corresponding authors.
E-mail addresses: szwang@yahoo.cn (C. Wang), Qsli@scnu.edu.cn (Q. Li).

2210-271X/$ - see front matter © 2012 Elsevier B.V. All rights reserved.
http://dx.doi.org/10.1016/j.comptc.2012.04.011

neutralization of its cation radical, studied the potential energy surface of singlet [C, H_3, N and O] system theoretically by the G2(MP2) method and proved the remarkable stability of CH_2=N(H)—O [42]. Aminova and Ermakova investigated two rearrangement pathways from singlet CH_2=N(H)—O to $OC(H)NH_2$ by quantum mechanics and molecular mechanics methods [43] which contain oxygen transfer process and proton transfer process. Yang et al. studied the title reaction system by MP2 (full) as well as B3LYP methods, and their attention was mainly paid on the addictive reaction pathways in which O atom is added to the carbon or nitrogen atom. They gave the reaction barriers of the corresponding reaction channels, and predicted three stable triplet addictive products, OCH_2NH (C_s), CH_2NHO (C_1) and CH_3NO (C_s) [3].

However, to our best knowledge, the rate constants for the H-abstraction reaction of the title system cannot be directly measured by experiment, and available theoretical investigations are rare to the above H-abstraction processes. It is desirable to inspect their kinetic behavior, which is helpful to understand the details in many atmosphere and combustion reactions. To achieve the full mechanism of the title reaction system, more possible reaction pathways should be considered. In the present work, dual-level direct dynamics method [44–48] is carried out on the title reaction system to obtain the minimum energy path (MEP) information. The rate constants are calculated using conventional transition state theory (TST) and variational transition state theory (VTST) methods. The tunneling effect is taken into account. Calculated rate constants of the H-abstraction reaction pathways are compared with the experimental data at a wide temperature range from 200 to 2500 K.

2. Calculation methods

The electronic structure calculations are performed by Gaussian 03 program [49]. The geometrical parameters of the stationary points including reactants, intermediates, products and transition states are obtained at the QCISD/cc-pVDZ level. QCISD [50] denotes Quadratic Configuration Interaction including Single and Double substitution, and cc-pVDZ refers to the Dunning's correlation consistent basis set including double-ζ [51]. The harmonic vibrational frequencies of stationary structures are also calculated at the same level. Number of imaginary frequencies can be used to confirm the type of the stationary point, 0 for a local minima and 1 for a saddle point. From the frequency analysis, zero-point energy (ZPE) can be obtained. Minimum energy paths (MEPs) are confirmed by intrinsic reaction coordinate (IRC) theory [52] at the same level, with a gradient step-size of 0.03 $(amu)^{1/2}$ bohr. To achieve more reliable potential energy information, a more accurate calculation are performed at the QCISD(T)/aug-cc-pVTZ level to refine the single point energy of the structures optimized at the QCISD/cc-pVDZ level. QCISD(T) means Quadratic CI calculation including single and double substitutions with a triples contribution to the energy added [50], and aug-cc-pVTZ [51] denotes the Dunning's correlation consistent basis set including triple-ζ and with additional diffuse functions.

By means of POLYRATE 9.4 program package [53], rate constants are calculated by conventional transition state theory (TST) [54] and improved canonical variational transition state theory (ICVT) [55] methods incorporating small-curvature tunneling (SCT) [56,57] effect using the single point energy, gradient and

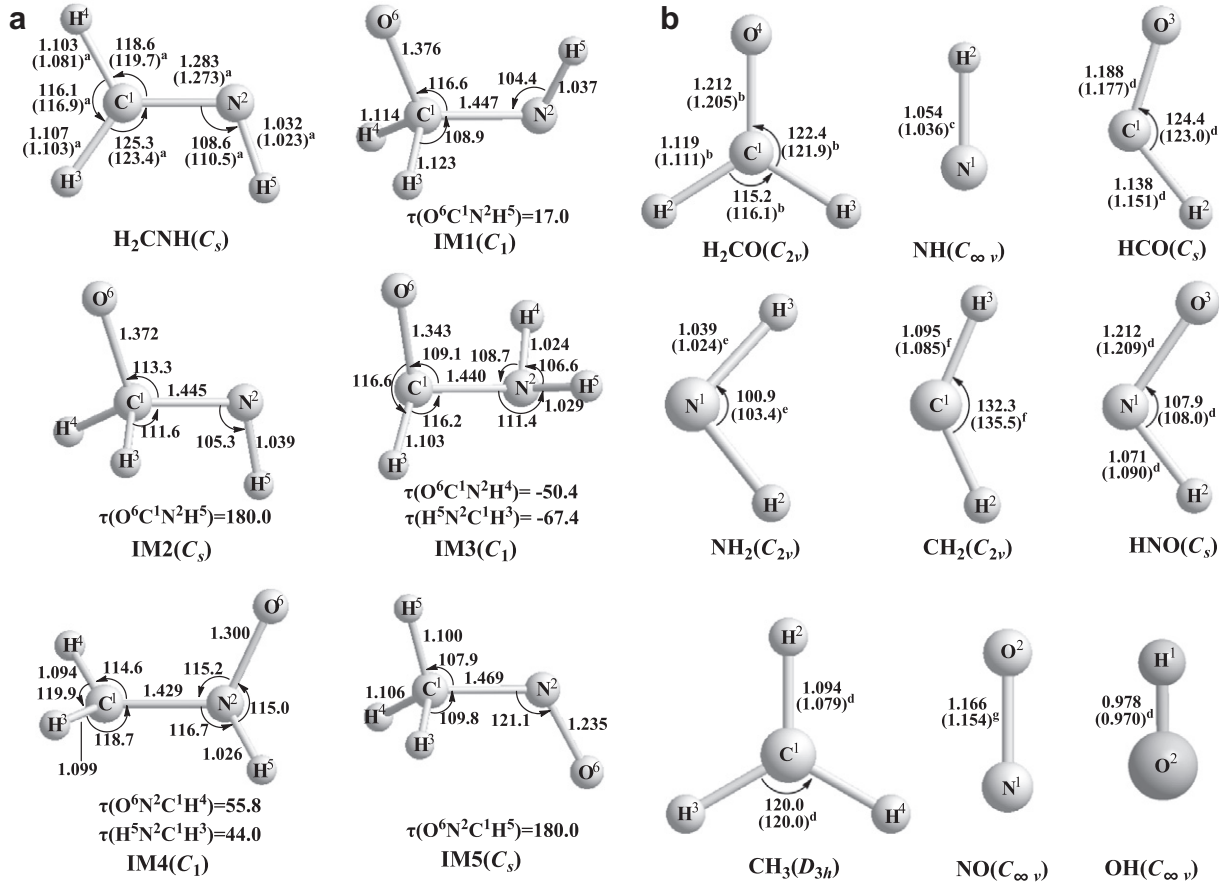

Fig. 1. Conformations of reactants, products, intermediates (IMs) and transition states (TSs) for the title reaction at QCISD/cc-pVDZ level. The bond distances are in angstrom and the angles and diangles are in degree respectively. *a*, *b*, *c*, *d*, *e*, *f*, and *g* are from Refs. [58–64] respectively.

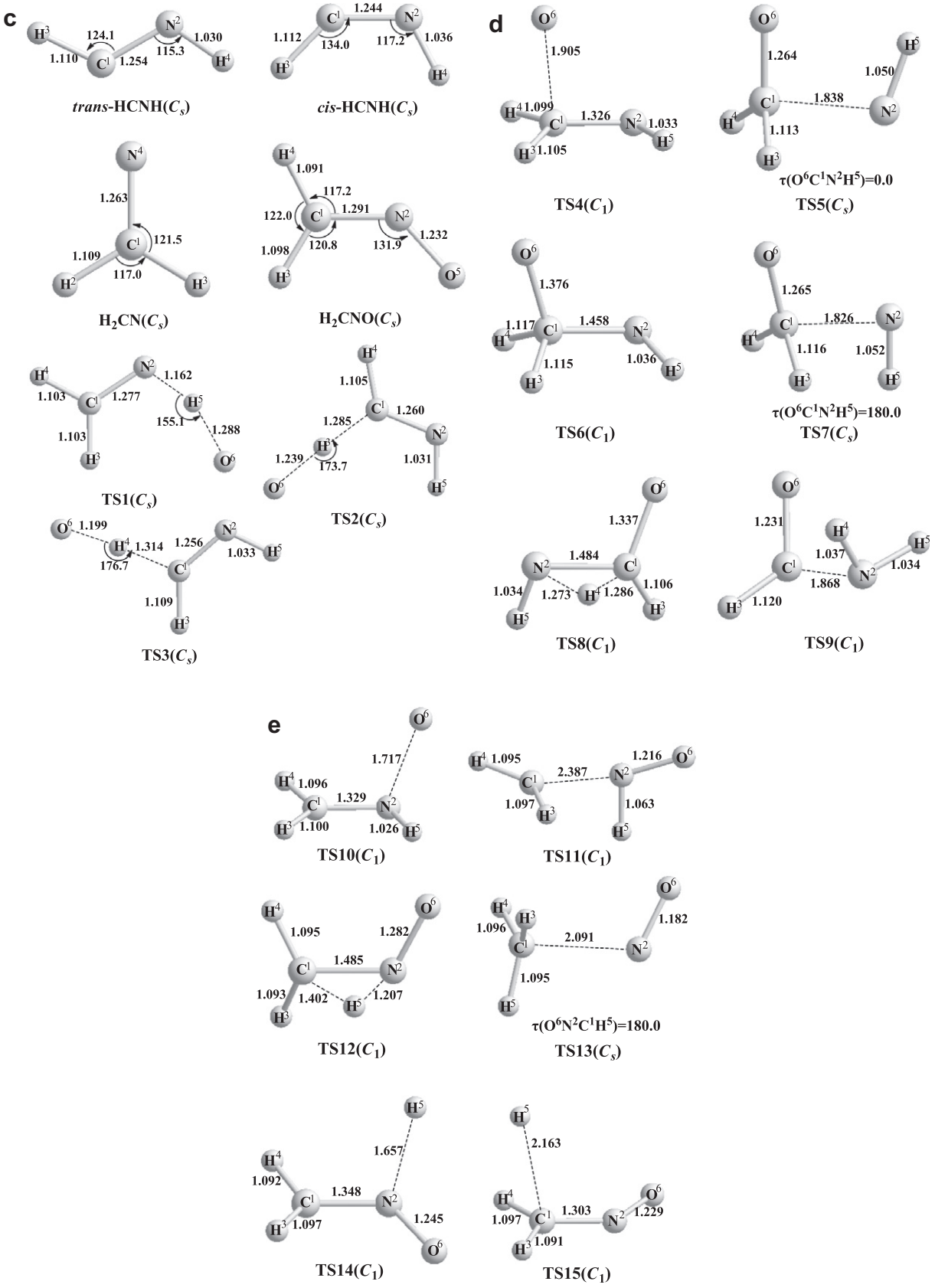

Fig. 1 (*continued*)

Hessian information of the corresponding reactants, products, transition states and some points along the MEP obtained by dual-level calculations. The spin-orbit splitting of $O(^3P)$, which is 158.5 and 226.5 cm^{-1} for $^3P_0$ and $^3P_1$ relative to $^3P_2$, and of OH,

which is 140.0 cm^{-1} for $^2\Pi_{1/2}$ relative to $^2\Pi_{3/2}$, are considered when calculating the electronic partition functions. The rate constants are evaluated in the wide temperature range of 200–2500 K. The Euler single-step integrator with a step size of 0.001 $(amu)^{1/2}$ bohr is used to follow the MEP, and the generalized normal mode analysis is carried out in every 0.05 $(amu)^{1/2}$ bohr.

3. Result and discussion

3.1. Geometries, frequencies and schematic potential energy surface

The optimized geometrical structures including reactants, products, intermediates and transition states of the title reaction system at the QCISD/cc-pVDZ level are shown in Fig. 1 [58–64]. It can be seen that the bond lengths and bond angles obtained theoretically are consistent with the experimental data. The largest deviations of the bond length and the bond angle are 0.022 Å (2.0%) for C^1—H^4 of H_2CNH and 3.2° (2.4%) for ∠HNH of NH_2, respectively.

In Fig. 2, the potential energy information of the title reaction system is presented. The relative energies are given by setting the sum of the single point energies of the reactants H_2CNH and O to be zero as reference. From Fig. 2, it can be found that two types of reactions are presented. The H-abstraction type reaction includes three pathways, and adduct-decomposition type reaction contains seven pathways. The all reaction pathways are shown as follows:

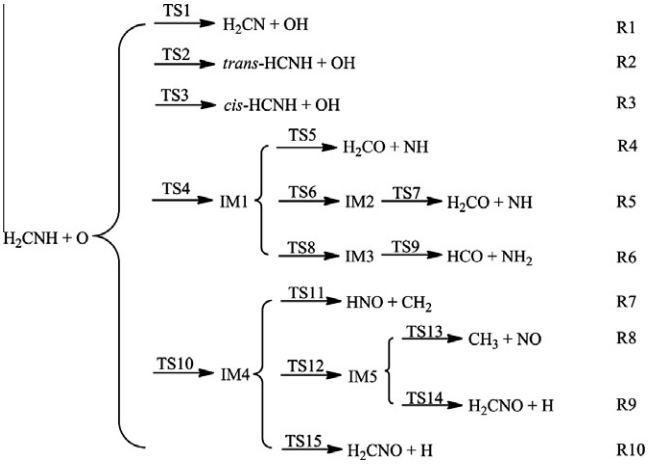

The frequencies of all stationary points for the title reaction system are obtained at the QCISD/cc-pVDZ level (Table 1) [60,62,65–73]. Generally, the theoretical frequency values are in agreement with the experimental data and the deviations are within 10%, except for the lowest frequency 404 cm^{-1} of CH_3. The corresponding experimental frequency value of CH_3 is 606 cm^{-1}. But in previous theoretical frequency analysis, Yu et al. predicted the frequency of the same vibrational mode to be 434 cm^{-1} at UQCISD/6-311G(d,p) level [74] and Jing et al. calculated the same frequency to be 418 cm^{-1} at MP2/6-311G(d,p) level and 503 cm^{-1} at B3LYP/6-311G(d,p) level [75]. All the transition state structures have only one imaginary frequency, and they are confirmed by IRC method to connect with the reactants and products of every elementary reaction. The imaginary frequency values of the transition states of three H-abstraction reactions fall into the range of 2095*i*–2200*i* cm^{-1}, which suggests that the tunneling effect in calculating the rate constants will be significant.

3.1.1. H-abstraction reaction pathways

Three H-abstraction pathways (R1–R3) have been studied. R1 has the lowest barrier height (4.53 kcal/mol for TS1) of the ten

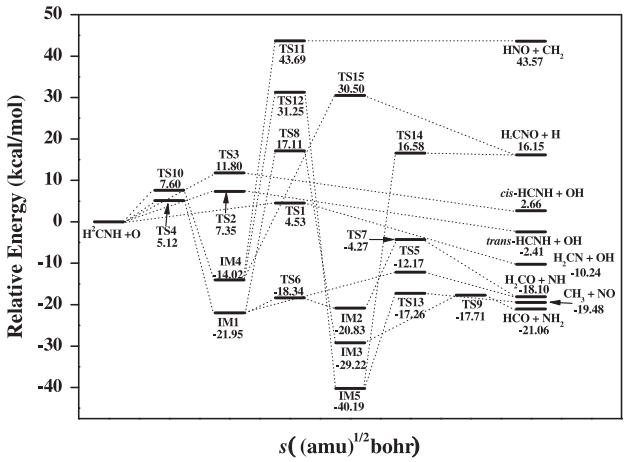

Fig. 2. Potential energy information (kcal/mol) of all stationary points including Reactants, Products, Intermediates (IMs), and Transition states (TSs) for the title reaction system at the QCISD(T)/aug-cc-pVTZ//QCISD/cc-pVDZ level.

reaction pathways (R1–R10) and a favored reaction energy (−10.2 kcal/mol for H_2CN + OH). At 298 K, the computed standard reaction enthalpy (−11.6 kcal/mol) is in good agreement with the experimental data (−11.1 kcal/mol) (Table 2) [4,76]. The N—H bond distance in TS1 increases 13% relative to the corresponding bond distance in H_2CNH, and the O—H bond distance in TS1 increases 32% than that in the product OH. The transition state is obviously reactant-like. So the negative reaction energy value can be expected according to the Hammond Postulate [77]. R1 is considered to be the most favored reaction pathway of the title reaction system. R2 and R3 are H-abstraction reactions from the carbon atom. R2 has lower barrier height (7.35 kcal/mol for TS2) and smaller reaction energy (−2.41 kcal/mol for *trans*-HCNH) than R3 (11.80 kcal/mol for TS3 and 2.66 kcal/mol for *cis*-HCNH). For R2, the theoretical reaction enthalpy, −4.2 kcal/mol, is also comparable to the experimental value of −5.9 kcal/mol. The transition state structures of above three H-abstraction reactions are of C_s symmetry, which indicates that oxygen atom attacks every hydrogen atom of H_2CNH along the molecule plane. IRC calculations also suggest that the three H-abstraction reactions occur in the molecule plane.

3.1.2. Adduct-decomposition reaction pathways

Another important entrance for oxygen atom towards H_2CNH is attacking the carbon atom, which leads to three reaction pathways. The oxygen atom adds to the carbon atom forming the C_1 intermediate IM1 (−21.95 kcal/mol) with the barrier height of 5.12 kcal/mol (TS4). IM1 is theoretically optimized to be a C_s structure at MP2(full)/aug-cc-pVDZ level by Yang et al [3]. But in this work, the C_s structure has an imaginary frequency of 955*i* at QCISD/cc-pVDZ level. After following the corresponding normal mode, the C_1 IM1 without imaginary frequencies is energetically ~0.6 kcal/mol lower than the C_s structure with one imaginary frequency. From IM1 to the product H_2CO and NH, there are two reaction pathways (R4 and R5). For R4, IM1 decomposes into the products H_2CO and NH, over the transition state TS5 with the barrier height of 9.78 kcal/mol (E_{TS5}–E_{IM1}). R5 is composed by two steps of elementary reactions. The first elementary reaction is an isomerization process from IM1 to IM2 via TS6 with a relatively low barrier height of 3.61 kcal/mol (E_{TS6}–E_{IM1}). The second one is a dissociation reaction in which the C—N bond is elongated to form the products H_2CO and NH with the barrier height of 16.56 kcal/mol (E_{TS7}–E_{IM2}). IM2 overleaps TS8 with the high barrier height 39.06 kcal/mol (E_{TS8}–E_{IM1}) to form IM3, a very stable species which is energetically −29.22 kcal/mol lower than the reactants. Then the

Table 1
The harmonic vibrational frequencies (cm^{-1}) and zero-point energies (*ZPEs*) (kcal/mol) of reactants, products, intermediates and transition states at the QCISD/cc-pVDZ level of theory.

Species	Frequencies	ZPE*
H_2CNH	3437, 3172, 3067, 1708, 1489, 1394, 1168, 1078, 1076	25.1
	3263, 3024, 2914, 1638, 1452, 1344, 1127, 1061, 1058[a]	*24.1*
H_2CO	3004, 2944, 1816, 1544, 1275, 1193	16.8
	2843, 2782, 1746, 1500, 1249, 1167[b]	*16.1*
NH	3218	4.6
	3283[c]	*4.7*
HCO	2675, 1894, 1135	8.2
	2434, 1868, 1081[a]	*7.7*
NH_2	3436, 3342, 1571	11.9
	3301,[d] *3219,1497*[a]	*11.5*
CH_2	3376, 3152, 1129	11.0
	3190,[a]*2806,*[e]*963*[a]	*9.9*
HNO	2871, 1651, 1575	8.7
	2684, 1565,[a] *1501*[d]	*8.2*
CH_3	3324, 3324, 3132, 1416, 1416, 404	18.6
	3161, 3161, 3004, 1396, 1396, 606	*18.2*
NO	1885	2.7
	1904[f]	*2.7*
trans-HCNH	3459, 3064, 1781, 1229, 991, 931	16.4
	1218, 886[g]	
cis-HCNH	3343, 3014, 1821, 1063, 908, 888	15.8
H_2CN	3103, 3032, 1699, 1385, 981, 941	15.9
	3103,[h] *2820,*[i] *1725, 1337, 954, 913*[h]	
OH	3723	5.3
	3738[j]	*5.3*
CH_2NO	3312, 3163, 1712, 1500, 1222, 1136, 827, 733, 442	20.1
	1664, 1197,1104, 793[k]	
IM1	3402, 2998, 2882, 1384, 1350, 1201, 1114, 1080, 995, 769, 483, 210	25.5
IM2	3379, 2923, 2898, 1428, 1345, 1225, 1114, 1000, 999, 632, 540, 354	25.5
IM3	3568, 3445, 3123, 1649, 1300, 1207, 1166, 1080, 865, 789, 342, 244	26.8
IM4	3478, 3291, 3148, 1498, 1450, 1284, 1169, 1050, 701, 643, 431, 263	26.3
IM5	3197, 3130, 3050, 1570, 1478, 1477, 1420, 1130, 1080, 945, 403, 201	27.3
TS1	3194, 3097, 1714, 1432, 1354, 1132, 1074, 1047, 598, 464, 242, 2155*i*	21.9
TS2	3462, 3127, 1780, 1338, 1187, 1066, 1060, 977, 572, 380, 110, 2095*i*	21.5
TS3	3427, 3065, 1783, 1265, 1145, 1051, 1005, 943, 529, 337, 168, 2200*i*	21.0
TS4	3437, 3201, 3086, 1559, 1397, 1340, 1074, 1040, 981, 474, 254, 666*i*	25.5
TS5	3287, 3044, 2978, 1588, 1418, 1233, 1113, 921, 845, 359, 270, 630*i*	24.4
TS6	3399, 2982, 2939, 1415, 1353, 1295, 1096, 1057, 1014, 648, 467, 354*i*	25.3
TS7	3249, 3000, 2929, 1543, 1385, 1240, 962, 922, 722, 332, 256, 809*i*	23.6
TS8	3437, 3073, 2286, 1339, 1284, 1138, 1103, 923, 874, 598, 350, 2237*i*	23.5
TS9	3498, 3391, 2896, 1630, 1565, 1113, 940, 794, 701, 395, 229, 509*i*	24.5
TS10	3523, 3261, 3134, 1527, 1354, 1297, 1126, 989, 825, 457, 335, 779*i*	25.5
TS11	3354, 3138, 2949, 1588, 1506, 1144, 483, 271, 250, 171, 32, 289*i*	21.3
TS12	3317, 3165, 2220, 1404, 1253, 1226, 1063, 910, 755, 387, 315, 2180*i*	22.9
TS13	3304, 3296, 3119, 1715, 1428, 1427, 915, 582, 543, 266, 79, 460*i*	23.8
TS14	3315, 3166, 1483, 1361, 1161, 1111,789, 669, 614, 570, 328, 1681*i*	20.8
TS15	3318, 3169, 1652, 1495, 1211, 1132, 824, 756, 444, 333, 223, 574*i*	20.8

a, *b*, *c*, *d*, *e*, *f*, *g*, *h*, *i*, *j*, *k* are from Refs. [65–67,60,68–72,62,73], respectively.
* ZPE (*Italic*): from http://webbook.nist.gov/chemistry.

C—N bond is elongated and finally broken up to form HCO and NH_2 via TS9 with a barrier height of 11.51 kcal/mol (E_{TS9}–E_{IM3}). The

Table 2
The reaction energy, classical barrier height (kcal/mol) and reaction enthalpy (298.15 K, kcal/mol) at the QCISD(T)/aug-cc-pVTZ//QCISD/cc-pVDZ level of theory for R1 and R2.

Pathway	ΔE	$V^{\neq b}$	$\Delta H^{\theta}_{298.15\ K}$	*Expt*
R1	−10.2	4.5	−11.6	−11.1[a]
R2	−2.4	7.3	−4.2	−5.9[b]

[a] From Ref. [4].
[b] From Ref. [76].

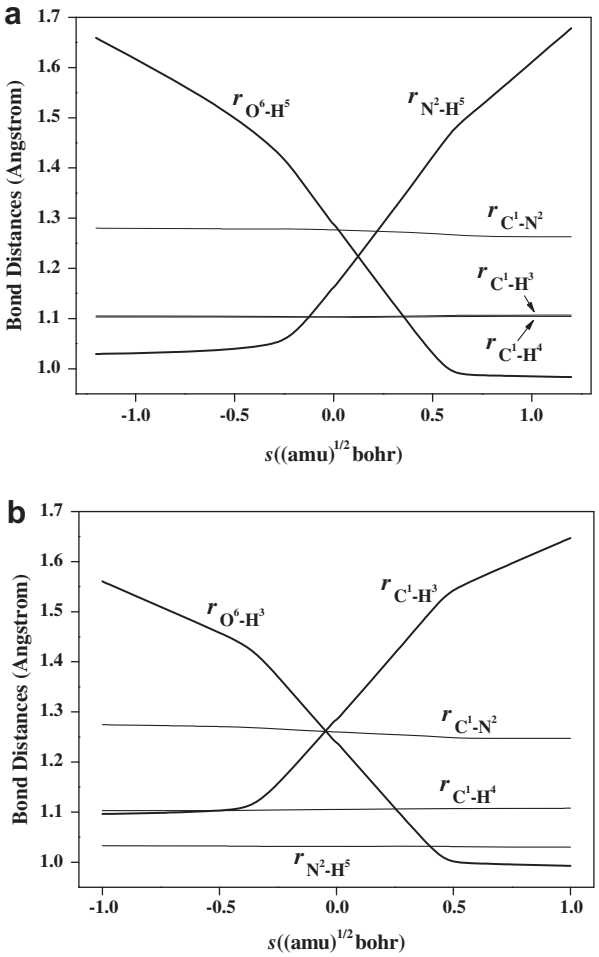

Fig. 3. Changes of the bond distances (Å) as functions of *s* ($(amu)^{1/2}$ bohr) at the QCISD/cc-pVDZ level for R1 (a) and R2 (b).

relative energy of the product ($HCO + NH_2$) is the lowest (−21.06 kcal/mol). The reaction energy is favored, but the barrier height of the reaction IM1 → IM3 via TS8 is relatively large.

Attacking nitrogen atom is another entrance for the oxygen atom, directly forming the stable additive intermediate IM4 (−14.02 kcal/mol) via TS10 over the barrier height of 7.60 kcal/mol. The three transition states (TS11, TS12, and TS15) after IM4 connecting to three types of products ($HNO + CH_2$, $CH_3 + NO$, and $H_2CNO + H$) via four reaction pathways (R7-R10) are high lying (Fig. 2). When the C—N bond is stretched, not only the transition state (TS11), but also the products of R7 ($HNO + CH_2$) is energetically over 30 kcal/mol higher than the reactants. For R8, though the global minimum IM5 (−40.19 kcal/mol) and the products (−19.48 kcal/mol for $CH_3 + NO$) are low lying, the barrier height is still as high as 45.27 kcal/mol in the elementary reaction IM4 → IM5 via TS12. Products H_2CNO and H can be obtained along

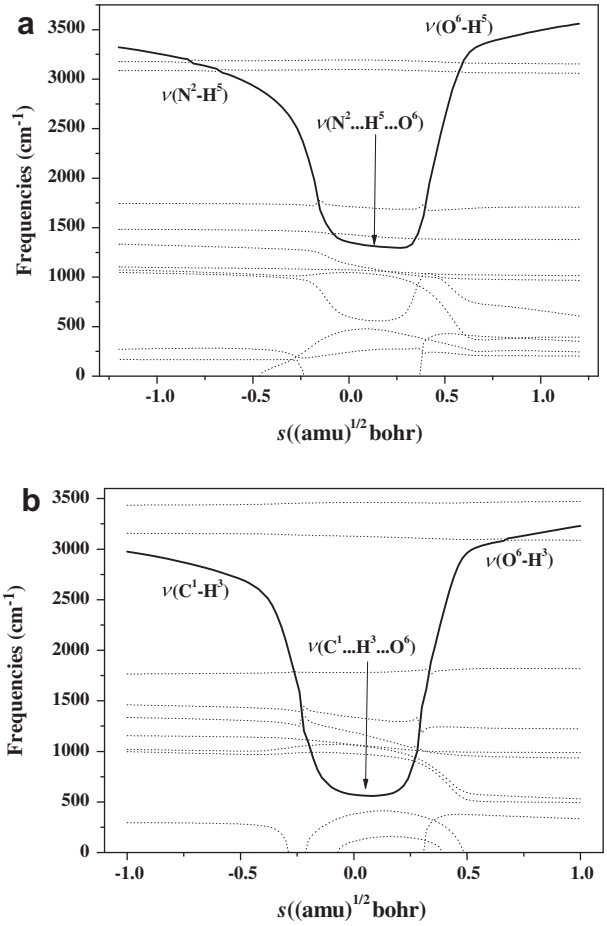

Fig. 4. Changes of the generalized normal-mode vibrational frequencies (cm^{-1}) as functions of s ((amu)$^{1/2}$ bohr) at the QCISD/cc-pVDZ level for R1 (a) and R2 (b).

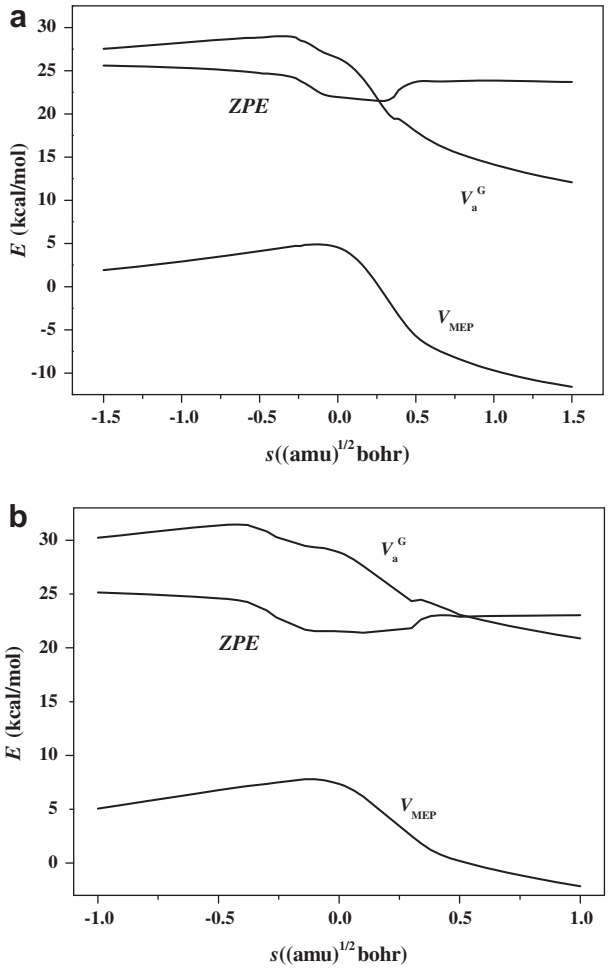

Fig. 5. Classical potential energy (V_{MEP}), zero-point energy (ZPE) and ground-state vibrational adiabatic potential energy (V_a^G) (kcal/mol) as functions of s ((amu)$^{1/2}$ bohr) at the QCISD(T)/aug-cc-pVTZ//QCISD/cc-pVDZ level for R1 (a) and R2 (b).

two reaction pathways R9 and R10. However, the corresponding barrier heights are over 30 kcal/mol (TS14 and TS15).

3.2. Calculations of rate constants

The rate constants of the two H-abstraction reaction pathways, R1 and R2, are discussed detailed in this section.

Fig. 3 shows the changes of bond distances along the MEP as a function of reaction coordinate s at the QCISD/cc-pVDZ level. For R1 (Fig. 3a), the bond distances of N^2—H^5 and O^6—H^5 change significantly over the whole reaction process, especially in the range of $-0.25 < s < 0.6$ ((amu)$^{1/2}$ bohr). In this range, the N^2—H^5 bond distance elongates from ~1.06 Å to ~1.5 Å, and the O^6—H^5 bond distance shortens to ~1.0 Å from ~1.4 Å. Above changes indicate the process of breaking of the N—H bond and forming of the O—H bond, namely the H-abstraction reaction mainly take place in the range of $-0.25 < s < 0.6$ (amu)$^{1/2}$ bohr. The rest bond distances of the reaction system are almost unchanged along the MEP. Similar to R1, R2 (Fig. 3b) is a process of forming of the O^6—H^3 bond and breaking of the C^1—H^3 bond, which occurs in the range of $-0.4 < s < 0.5$ (amu)$^{1/2}$ bohr.

Changes of frequencies as the function of reaction coordinate s along the MEP for R1 and R2 at QCISD/cc-pVDZ level are presented in Fig. 4. For R1 (Fig. 4a), in the negative and positive limits of reaction coordinate s, the frequencies are associated with the reactants and the products respectively. The solid line shows that the N^2—H^5 stretching vibrational frequency decreases and the O^6—H^5 stretching vibrational frequency increases gradually along the MEP. It also suggests a process of breaking of the N—H bond and forming of the O—H bond. Other vibrational frequency values do not change obviously. Similarly, a reaction of breaking the C—H bond and forming the O—H bond are depicted for R2 (Fig. 4b).

The classical potential energy (V_{MEP}), vibrationally adiabatic ground-state potential energy (V_a^G), and zero-point energy (ZPE) curves of R1 and R2 as functions of the reaction coordinate s are presented in Fig. 5a and b, respectively, at the QCISD(T)/aug-cc-pVTZ//QCISD/cc-pVDZ level. For both reaction pathways R1 and R2, the $V_{MEP}(s)$ and the $V_a^G(s)$ energy curves are similar in shape. The ZPE curves of R1 and R2 have some lower values near transition state ($s = 0$ (amu)$^{1/2}$ bohr) as the common H-abstraction reactions. To further study the variational effect in calculating the rate constants for R1 and R2, the bottleneck properties of R1 and R2 based on the canonical variational transition state theory are listed in Tables 3 and 4 respectively. The bottleneck properties indicate the positions of the variational transition state deviated from the saddle point ($s = 0.0$ (amu)$^{1/2}$ bohr) at various temperatures. For R1 (Table 3), the largest deviation in the temperature range 200–2500 K appears at 200 K, at which $s = -0.313$ (amu)$^{1/2}$ bohr, $\Delta V_{MEP} = V_{MEP}\ (s = -0.313) - V_{MEP}\ (s = 0.000) = 0.08$ (kcal/mol), $\Delta V_a^G = V_a^G\ (s = -0.313) - V_a^G\ (s = 0.000) = 2.05$ (kcal/mol). And for R2 (Table 4), the largest deviation in the temperature range 200–2500 K emerges at 273 K, at which $s = -0.031$ (amu)$^{1/2}$ bohr, $\Delta V_{MEP} = V_{MEP}\ (s = -0.031) - V_{MEP}\ (s = 0.000) = 0.22$ (kcal/mol), $\Delta V_a^G = V_a^G\ (s = -0.031) - V_a^G\ (s = 0.000) = 0.25$ (kcal/mol). The

Table 3
Bottleneck properties for R1.

T (K)	s ((amu)$^{1/2}$ bohr)	V_{MEP} (kcal/mol)	V_a^G (kcal/mol)
SP	0.000	4.53	26.47
200	−0.313	4.61	28.52
273	−0.298	4.65	28.49
373	−0.280	4.69	28.44
500	−0.264	4.73	28.39
800	−0.237	4.79	28.21
1273	−0.207	4.83	27.94
1600	−0.198	4.85	27.85
2000	−0.191	4.85	27.79
2500	−0.188	4.86	27.75

Table 4
Bottleneck properties for R2.

T (K)	s ((amu)$^{1/2}$ bohr)	V_{MEP} (kcal/mol)	V_a^G (kcal/mol)
SP	0.000	7.35	28.87
200	−0.028	7.55	29.09
273	−0.031	7.57	29.12
373	0.027	7.38	28.91
500	0.026	7.38	28.91
800	0.025	7.38	28.91
1273	0.026	7.38	28.91
1600	0.028	7.37	28.90
2000	0.029	7.37	28.90
2500	0.031	7.36	28.89

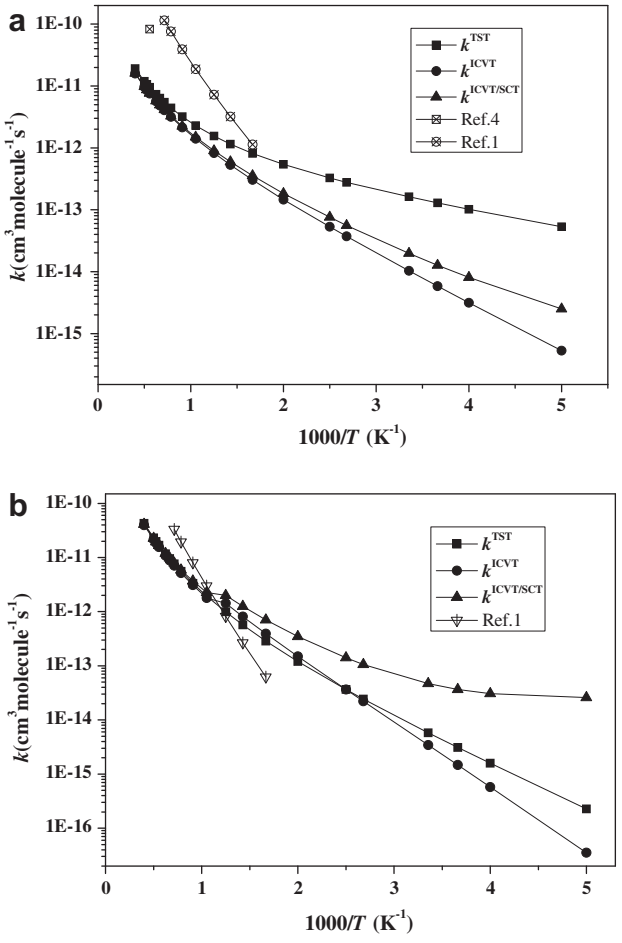

Fig. 6. Plot of the TST, ICVT and ICVT/SCT rate constants (cm^3 molecule^{-1} s^{-1}) at the QCISD(T)/aug-cc-pVTZ//QCISD/cc-pVDZ level versus 1000/T (K^{-1}) in the temperature range of 200–2500 K for R1 (a) and R2 (b).

Table 5
The TST, ICVT and ICVT/SCT rate constants, k (cm^3 molecule^{-1} s^{-1}), calculated at the QCISD(T)/aug-cc-pVTZ//QCISD/cc-pVDZ level for R1 between 200 and 2500 K and some available experimental results.

T (K)	TST	ICVT	ICVT/SCT	Ref. [4]	Ref. [1]
200	5.33E-14	5.28E-16	2.49E-15		
250	1.02E-13	3.15E-15	8.09E-15		
273	1.29E-13	5.82E-15	1.27E-14		
298	1.62E-13	1.03E-14	1.97E-14		
373	2.77E-13	3.71E-14	5.60E-14		
400	3.26E-13	5.30E-14	7.57E-14		
500	5.41E-13	1.46E-13	1.83E-13		
600	8.15E-13	3.03E-13	3.55E-13		1.13E-12
700	1.15E-12	5.29E-13	5.94E-13		3.20E-12
800	1.55E-12	8.24E-13	9.01E-13		7.24E-12
950	2.29E-12	1.40E-12	1.49E-12		1.87E-11
1100	3.19E-12	2.13E-12	2.23E-12		3.90E-11
1273	4.42E-12	3.16E-12	3.27E-12		7.63E-11
1400	5.47E-12	4.04E-12	4.16E-12		1.15E-10
1500	6.38E-12	4.81E-12	4.93E-12		
1600	7.35E-12	5.64E-12	5.77E-12		
1800	9.51E-12	7.51E-12	7.64E-12	8.29E-11	
1900	1.07E-11	8.53E-12	8.67E-12		
2000	1.19E-11	9.62E-12	9.76E-12		
2500	1.91E-11	1.59E-11	1.61E-11		

Table 6
The TST, ICVT and ICVT/SCT rate constants, k (cm^3 molecule^{-1} s^{-1}), calculated at the QCISD(T)/aug-cc-pVTZ//QCISD/cc-pVDZ level for R2 between 200 and 2500 K and some available experimental results.

T (K)	TST	ICVT	ICVT/SCT	Ref. [1]
200	2.27E-16	3.54E-17	2.58E-14	
250	1.58E-15	5.76E-16	3.05E-14	
273	3.10E-15	1.47E-15	3.66E-14	
298	5.80E-15	3.43E-15	4.68E-14	
373	2.43E-14	2.21E-14	1.06E-13	
400	3.65E-14	3.66E-14	1.41E-13	
500	1.20E-13	1.49E-13	3.49E-13	
600	2.87E-13	3.92E-13	7.07E-13	6.22E-14
700	5.68E-13	8.09E-13	1.25E-12	2.66E-13
800	9.90E-13	1.43E-12	2.00E-12	8.21E-13
950	1.94E-12	1.78E-12	2.26E-12	2.99E-12
1100	3.34E-12	3.09E-12	3.69E-12	8.01E-12
1273	5.56E-12	5.17E-12	5.90E-12	1.94E-11
1400	7.65E-12	7.11E-12	7.94E-12	3.31E-11
1500	9.57E-12	8.90E-12	9.80E-12	
1600	1.17E-11	1.09E-11	1.19E-11	
1800	1.68E-11	1.57E-11	1.68E-11	
1900	1.98E-11	1.84E-11	1.96E-11	
2000	2.30E-11	2.14E-11	2.26E-11	
2500	4.26E-11	3.98E-11	4.12E-11	

comparison of bottleneck properties between R1 and R2 implies that the variational effect of R1 may be bigger than that of R2.

The forward rate constants of R1 and R2 at the wide temperature range of 200–2500 K are calculated by TST and ICVT methods using POLYRATE 9.4 program package (Fig. 6). For R1 (Fig. 6a, Table 5) [1,4], it can be seen that the theoretical rate constants are close to the available experimental values in the corresponding experimental temperature ranges with small deviations. The rate constants of TST and ICVT methods are of significant difference below 1000 K, which indicates the large variational effect for R1. And in the low temperature range (below 300 K), the rate constant by the ICVT/SCT method is bigger than that by ICVT method by a factor of 2 or more. So the tunneling effect correction cannot be neglected in calculating the rate constants at low temperature range. The theoretical rate constants of R1 by the ICVT/SCT method are fitted by the three-parameter expression in units of cm^3 molecule^{-1} s^{-1} as $k = 1.64 \times 10^{-17} T^{1.81} \exp(-962.61/T)$. For R2, as described in Fig. 6b and Table 6, the theoretical rate constants

are also close to the available experimental results at the temperature range from 600 to 1400 K. The rate constants by TST and ICVT methods are nearly the same. So the variational effect correction is small in the calculations of rate constants at the corresponding temperature range. It can be seen from Fig. 6b and Table 6 that the tunneling effect is significant at low temperature range. The theoretical rate constants by ICVT/SCT method are expressed as $k = 2.98 \times 10^{-19}\, T^{2.43} \exp(-692.65/T)\ \mathrm{cm^3\ molecule^{-1}\ s^{-1}}$.

4. Conclusion

In this work, the mechanisms for the multi-pathway reaction system of H_2CNH and $O(^3P)$ have been investigated at the QCISD(T)/aug-cc-pVTZ//QCISD/cc-pVDZ level. The two favored H-abstraction reaction pathways, R1 and R2, are identified and studied in detail. The barrier heights of R1 and R2 are 4.53 and 7.35 kcal/mol, respectively. The theoretically calculated results show that the variational effect is considerable for R1, while small for R2. At low temperature range, the tunneling effect corrections play an important role for calculations of rate constants of R1 and R2. Rate constants of R1 and R2 are obtained by the TST, ICVT, and ICVT/SCT methods, which are close to the available experimental values in the wide temperature ranges. The three-parameter fitted rate constants by the ICVT/SCT method for R1 and R2 within 200–2500 K are respectively expressed as:

$$k_{R1} = 1.64 \times 10^{-17}\ T^{1.81} \exp(-962.61/T)\ \mathrm{cm^3\ molecule^{-1}\ s^{-1}}$$

And

$$k_{R2} = 2.98 \times 10^{-19}\ T^{2.43} \exp(-692.65/T)\ \mathrm{cm^3\ molecule^{-1}\ s^{-1}}.$$

Acknowledgements

Thanks to Professor D.G. Truhlar for providing the POLYRATE 9.4 program. This work is supported by the National Natural Science Foundation of China (20973066).

References

[1] M.V. Kantak, K.S. De Manrique, R.H. Aglave, R.P. Hesketh, Methylamine oxidation in a flow reactor: mechanism and modeling, Combust. Flame 108 (1997) 235–265.
[2] B.A. Williams, J.W. Fleming, Radical species profiles in low-pressure methane flames containing fuel nitrogen compounds, Combust. Flame 110 (1997) 1–13.
[3] L.J. Yang, L.P. Meng, Y.L. Zeng, S.J. Zheng, Quantum chemistry and electron density topological study on the reaction of $CH_2NH(s)$ with O_3P atom, Acta Phys. Chim. Sin. 23 (2007) 311–316.
[4] J. Tomeczek, B. Gradoń, The role of N_2O and NNH in the formation of NO via HCN in hydrocarbon flames, Combust. Flame 133 (2003) 311–322.
[5] J.T. Herron, Evaluated chemical kinetic data for the reactions of atomic oxygen $O(^3P)$ with saturated organic compounds in the gas phase, J. Phys. Chem. Ref. Data 17 (1988) 967–1026.
[6] R. Atkinson, D.L. Baulch, R.A. Cox, J.N. Crowley, R.F. Hampson, R.G. Hynes, M.E. Jenkin, M.J. Rossi, J. Troe, Evaluated kinetic and photochemical data for atmospheric chemistry: volume I – gas phase reactions of O_x, HO_x, NO_x and SO_x species, Atmos. Chem. Phys. 4 (2004) 1461–1738.
[7] R. Atkinson, D.L. Baulch, R.A. Cox, J.N. Crowley, R.F. Hampson, R.G. Hynes, M.E. Jenkin, M.J. Rossi, J. Troe, Evaluated kinetic and photochemical data for atmospheric chemistry: volume II – gas phase reactions of organic species, Atmos. Chem. Phys. 6 (2006) 3625–4055.
[8] R. Atkinson, D.L. Baulch, R.A. Cox, J.N. Crowley, R.F. Hampson, R.G. Hynes, M.E. Jenkin, M.J. Rossi, J. Troe, Evaluated kinetic and photochemical data for atmospheric chemistry: volume III – gas phase reactions of inorganic halogens, Atmos. Chem. Phys. 7 (2007) 981–1191.
[9] R. Atkinson, D.L. Baulch, R.A. Cox, J.N. Crowley, R.F. Hampson, R.G. Hynes, M.E. Jenkin, M.J. Rossi, J. Troe, T.J. Wallington, Evaluated kinetic and photochemical data for atmospheric chemistry: volume IV – gas phase reactions of organic halogen species, Atmos. Chem. Phys. 8 (2008) 4141–4496.
[10] L.M. Reynard, D.J. Donaldson, OH production from the reaction of vibrationally excited H_2 in the mesosphere, Geophys. Res. Lett. 28 (2001) 2157–2160.
[11] H.D. Hartough, J.W. Schick, J.J. Dickert Jr., Aminomethylation of thiophene. V. The 2-thenylaminomethylsulfonic acids. The mechanism of the aminomethylation reaction, J. Am. Chem. Soc. 72 (1950) 1572–1577.
[12] R.D. J Godfrey, R.D. Brown, B.J. Robinson, M.W. Sinclair, Discovery of interstellar methanimine (formaldimine), Astrophys. Lett. 13 (1973) 119–121.
[13] J.E. Dickens, W.M. Irvine, C.H. DeVries, M. Ohishi, Hydrogenation of interstellar molecules: a survey for methylenimine (CH_2NH), Astrophys. J. 479 (1997) 307–312.
[14] C.J. Salter, T. Ghosh, B. Catinella, M. Lebron, M.S. Lerner, R. Minchin, E. Momjian, The Arecibo Arp 220 spectral census I: discovery of the pre-biotic molecule methanimine and new cm-wavelength transitions of other molecules, Astron. J. 136 (2008) 389–413.
[15] D.R. Johnson, F.J. Lovas, Microwave detection of the molecular transient methyleneimine (CH_2=NH), Chem. Phys. Lett. 15 (1972) 65–68.
[16] R. Pearson Jr., F.J. Lovas, Microwave spectrum and molecular structure of methylenimine (CH_2NH), J. Chem. Phys. 66 (1977) 4149–4156.
[17] D.E. Milligan, Infrared spectroscopic study of the photolysis of methyl azide and methyl-d_3 azlde in solid argon and carbon dioxide, J. Chem. Phys. 35 (1961) 1491–1497.
[18] M.E. Jacox, D.E. Milligan, The infrared spectrum of methylenimine, J. Mol. Spectrosc. 56 (1975) 333–356.
[19] C.B. Moore, G.C. Pimentel, T.D. Goldfarb, Matrix photolysis products of diazomethane: methyleneimine and hydrogen cyanide, J. Chem. Phys. 43 (1965) 63–70.
[20] Y. Hamada, K. Hashiguchi, M. Tsuboi, Y. Koga, S. Kondo, Pyrolysis of amines: infrared spectrum of methyleneimine, J. Mol. Spectrosc. 105 (1984) 70–80.
[21] G. Duxbury, H. Kato, M.L. Le Lerre, Laser Stark and interferometric studies of thioformaldehyde and methyleneimine, Faraday Discuss. Chem. Soc. 71 (1981) 97–110.
[22] L. Halonen, G. Duxbury, The Fourier transform infrared spectrum of methyleneimine in the 10 μm region, J. Chem. Phys. 83 (1985) 2078–2090.
[23] L. Halonen, G. Duxbury, High resolution infrared spectrum of methyleneimine, CH_2NH, in the 3 μm region, J. Chem. Phys. 83 (1985) 2091–2096.
[24] L. Halonen, G. Duxbury, Fourier transform infrared spectrum of CH_2NH: the $\nu 1$ band, Chem. Phys. Lett. 118 (1985) 246–251.
[25] C. Pouchan, K. Zaki, Ab initio configuration interaction determination of the overtone vibrations of methyleneimine in the region 2800–3200 $\mathrm{cm^{-1}}$, J. Chem. Phys. 107 (1997) 342–345.
[26] A. Teslja, B. Nizamov, P.J. Dagdigian, The electronic spectrum of methyleneimine, J. Phys. Chem. A 108 (2004) 4433–4439.
[27] M.J. Travers, D.C. Cowles, E.P. Clifford, G.B. Ellison, P.C. Engelking, Photoelectron spectroscopy of the CH_3N^- ion, J. Chem. Phys. 111 (1999) 5349–5360.
[28] L. Dore, L. Bizzocchi, C.D. Esposti, J. Gauss, The magnetic hyperfine structure in the rotational spectrum of H_2CNH, J. Mol. Spectrosc. 263 (2010) 44–50.
[29] C. Larson, Y. Ji, P. Samartzis, A.M. Wodtke, S.H. Lee, J.J.M. Lin, C. Chaudhuri, T.T. Ching, Collision-free photochemistry of methylazide: observation of unimolecular decomposition of singlet methylnitrene, J. Chem. Phys. 125 (2006) 133302.
[30] J.A. Pople, K. Raghavachari, M.J. Frisch, J.S. Binkley, P.v.R. Schleyer, Comprehensive theoretical study of isomers and rearrangement barriers of even-electron polyatomic molecules H_mABH_n (A, B=C, N, O, and F), J. Am. Chem. Soc. 105 (1983) 6389–6398.
[31] M.T. Nguyen, J. Rademakers, J.M.L. Martin, Concerning the heats of formation of the $[C, H_3, N]^+$ radical cations, Chem. Phys. Lett. 221 (1994) 149–155.
[32] M.T. Nguyen, D. Sengupta, T.K. Ha, Another look at the decomposition of methyl azide and methanimine: how is HCN formed?, J Phys. Chem. 100 (1996) 6499–6503.
[33] R. Sumathi, Dissociation and isomerization reactions of formaldimine on the ground and excited state surface, J. Mol. Struct. (THEOCHEM) 364 (1996) 97–106.
[34] J. Demuynck, D.J. Fox, Y. Yamaguchi, H.F. Schaefer, Triplet methylnitrene: an indefinitely stable species in the absence of collisions, J. Am. Chem. Soc. 102 (1980) 6204–6207.
[35] C. Gonzalez, H.B. Schlegel, Atmospheric chemistry of titan: ab initio study of the reaction between nitrogen atoms and methyl radicals, J. Am. Chem. Soc. 114 (1992) 9118–9122.
[36] C. Richards Jr., C. Meredith, S.J. Kim, G.E. Quelch, H.F. Schaefer, Is there a potential minimum corresponding to singlet methylnitrene? A study of the CH_3N to CH_2NH rearrangement on the lowest singlet state potential energy hypersurface, J. Chem. Phys. 100 (1994) 481–489.
[37] J.F. Arenas, J.I. Marcos, J.C. Otero, A. Sánchez-Gálvez, J. Soto, A multiconfigurational self-consistent field study of the thermal decomposition of methyl azide, J. Chem. Phys. 111 (1999) 551–561.
[38] C.R. Kemnitz, G.B. Ellison, W.L. Karney, W.T. Borden, CASSCF and CASPT2 ab initio electronic structure calculations find singlet methylnitrene is an energy minimum, J. Am. Chem. Soc. 122 (2000) 1098–1101.
[39] J. Roithová, D. Schröder, H. Schwarz, Unimolecular fragmentation of CH_3NH_2: towards a mechanistic description of HCN formation, Eur. J. Org. Chem. 15 (2005) 3304–3313.
[40] J. Zhou, H.B. Schlegel, Ab initio classical trajectory study of the dissociation of neutral and positively charged methanimine (CH_2NH^{n+} n = 0–2), J. Phys. Chem. A 113 (2009) 9958–9964.
[41] A.M. Dean, J.W. Bozzelli, Combustion chemistry of nitrogen, in: W.C. Gardiner Jr (Ed.), Gas-Phase Combustion Chemistry, Springer, New York, 2000, pp. 138–273.

[42] M. Polášek, F. Tureček, The elusive formaldonitrone, CH_2═N(H)─O. Preparation in the gas phase and characterization by variable-time neutralization-reionization mass spectrometry, and ab initio and density functional theory calculations, J. Am. Chem. Soc. 122 (2000) 525–531.
[43] R.M. Aminova, E. Ermakova, Rearrangements and proton transfer in nitrones by quantum chemistry and molecular dynamics, Chem. Phys. Lett. 359 (2002) 184–190.
[44] R.L. Bell, T.N. Truong, Direct ab initio dynamics studies of proton transfer in hydrogen-bond systems, J. Chem. Phys. 101 (1994) 10442–10451.
[45] T.N. Truong, W.T. Duncan, R.L. Bell, Direct ab initio dynamics methods for calculating thermal rates of polyatomic reactions, in: B.B. Laird, R.B. Ross, T. Ziegler (Eds.), Chemical Applications of Density Functional Theory, American Chemical Society, Washington, DC, 1996, pp. 85–104.
[46] D.G. Truhlar, D. Heidrich, The Reaction Path in Chemistry: Current Approaches and Perspectives, Kluwer, Dordrecht, The Netherlands, 1995.
[47] J.C. Corchado, J. Espinosa-Garcia, W.P. Hu, I. Rossi, D.G. Truhlar, Dual-level reaction-path dynamics (the /// approach to VTST with semiclassical tunneling). Application to OH + NH_3 → H_2O + NH_2, J. Phys. Chem. 99 (1995) 687–694.
[48] W.P. Hu, D.G. Truhlar, Factors affecting competitive ion-molecule reactions: ClO^- + C_2H_5Cl and C_2D_5Cl via E2 and S_N2 channels, J. Am. Chem. Soc. 118 (1996) 860–869.
[49] M.J. Frisch, G.W. Trucks, H.B. Schlegel, G.E. Scuseria, M.A. Robb, J.R. Cheeseman, J.A. Montgomery Jr, T. Vreven, K.N. Kudin, J.C. Burant, J.M. Millam, S.S. Iyengar, J. Tomasi, V. Barone, B. Mennucci, M. Cossi, G. Scalmani, N. Rega, G.A. Petersson, H. Nakatsuji, M. Hada, M. Ehara, K. Toyota, R. Fukuda, J. Hasegawa, M. Ishida, T. Nakajima, Y. Honda, O. Kitao, H. Nakai, M. Klene, X. Li, J.E. Knox, H.P. Hratchian, J.B. Cross, V. Bakken, C. Adamo, J. Jaramillo, R. Gomperts, R.E. Stratmann, O. Yazyev, A.J. Austin, R. Cammi, C. Pomelli, J.W. Ochterski, P.Y. Ayala, K. Morokuma, G.A. Voth, P. Salvador, J.J. Dannenberg, V.G. Zakrzewski, S. Dapprich, A.D. Daniels, M.C. Strain, O. Farkas, D.K. Malick, A.D. Rabuck, K. Raghavachari, J.B. Foresman, J.V. Ortiz, Q. Cui, A.G. Baboul, S. Clifford, J. Cioslowski, B.B. Stefanov, G. Liu, A. Liashenko, P. Piskorz, I. Komaromi, R.L. Martin, D.J. Fox, T. Keith, M.A. Al-Laham, C.Y. Peng, A. Nanayakkara, M. Challacombe, P.M.W. Gill, B. Johnson, W. Chen, M.W. Wong, C. Gonzalez, J.A. Pople, Gaussian 03, Revision E01, Gaussian, Inc., Wallingford, CT, 2004.
[50] J.A. Pople, M. Head-Gordon, K. Raghavachari, Quadratic configuration interaction. A general technique for determining electron correlation energies, J. Chem. Phys. 87 (1987) 5968–5975.
[51] T.H. Dunning Jr., Gaussian basis sets for use in correlated molecular calculations. I. The atoms boron through neon and hydrogen, J. Chem. Phys. 90 (1989) 1007–1023.
[52] K. Fukui, A formulation of the reaction coordinate, J. Phys. Chem. 74 (1970) 4161–4163.
[53] J.C. Corchado, Y.Y. Chuang, P.L. Fast, W.P. Hu, Y.P. Liu, G.C. Lynch, K.A. Nguyen, C.F. Jackels, A.F. Ramos, B.A. Ellingson, B.J. Lynch, V.S. Melissas, J. Villà, I. Rossi, E.L. Coitino, J.Z. Pu, T.V. Albu, R. Steckler, B.C. Garrett, A.D. Isaacson, D.G. Truhlar, POLYRATE version 94, Department of Chemistry and Supercomputer Institute, University of Minnesota, Minneapolis, Minnesota, 55455, 2006.
[54] S. Glasstone, K. Laidler, H. Eyring, The Theory of Rate Processes, McGraw-Hill, New York, 1941.
[55] B.C. Garrett, D.G. Truhlar, Improved canonical variational theory for chemical reaction rates. Classical mechanical theory and applications to collinear reactions, J. Phys. Chem. 84 (1980) 805–812.
[56] D.H. Lu, T.N. Truong, V.S. Melissas, G.C. Lynch, Y.P. Liu, B.C. Grarrett, R. Steckler, A.D. Issacson, S.N. Rai, G.C. Hancock, J.G. Lauderdale, T. Joseph, D.G. Truhlar, POLYRATE 4: A new version of a computer program for the calculation of chemical reaction rates for polyatomics, Comput. Phys. Commun. 71 (1992) 235–262.
[57] Y.P. Liu, G.C. Lynch, T.N. Truong, D.H. Lu, D.G. Truhlar, B.C. Garrett, Molecular modeling of the kinetic isotope effect for the [1,5] sigmatropic rearrangement of cis-1,3-pentadiene, J. Am. Chem. Soc. 115 (1993) 2408–2415.
[58] M.D. Harmony, V.W. Laurie, R.L. Kuczkowski, R.H. Schwendeman, D.A. Ramsay, F.J. Lovas, W.J. Lafferty, A.G. Maki, Molecular structures of gas-phase polyatomic molecules determined by spectroscopic methods, J. Phys. Chem. Ref. Data 8 (1979) 619–722.
[59] L.V. Gurvich, I.V. Veyts, C.B. Alcoc, Thermodynamic Properties of Individual Substances, fouth ed., Hemisphere Pub Co., New York, 1989.
[60] K.P. Huber, G. Herzberg, Molecular Spectra and Molecular Structure IV Constants of Diatomic Molecules, Van Nostrand Reinhold Co., 1979.
[61] J.F. Ogilvie, Structures of triatomic radicals HCO, HNO and HOO, J. Mol. Struct. 31 (1976) 407–410.
[62] G. Herzberg, Electronic Spectra and Electronic Structure of Polyatomic Molecules, Van Nostrand, New York, 1966.
[63] K. Kuchitsu, Structure of Free Polyatomic Molecules – Basic Data, Springer, Berlin, 1998.
[64] NIST Diatomic Spectral Database, <www.physicsnistgov/PhysRefData/MolSpec/Diatomic/index.html>.
[65] M.E. Jacox, Vibrational and electronic energy levels of polyatomic transient molecules, J. Phys. Chem. Ref. Data Monogr. 3 (1994) 1–461.
[66] T. Nakanaga, S. Kondo, S. Saëki, Infrared band intensities of formaldehyde and formaldehyde-d_2, J. Chem. Phys. 76 (1982) 3860–3865.
[67] K.K. Irikura, Experimental vibrational zero-point energies: diatomic molecules, J. Phys. Chem. Ref. Data 36 (2007) 389–397.
[68] D. Das, S.L. Whittenburg, Performance of the hybrid density functionals in the determination of the geometric structure, vibrational frequency and singlet–triplet energy separation of CH_2, CHF, CF_2, CCl_2 and CBr_2, J. Mol. Struct. (THEOCHEM) 492 (1999) 175–186.
[69] T. Shimanouchi, Tables of Molecular Vibrational Frequencies, Consolidated, vol. 1, NSRDS NBS-39.
[70] M.E. Jacox, Vibrational and electronic spectra of the H + HCN reaction products trapped in solid argon, J. Phys. Chem. 91 (1987) 6595–6600.
[71] M. Pettersson, J. Lundell, L. Khriachtchev, M. Räsänen, Neutral rare-gas containing charge-transfer molecules in solid matrices. III. HXeCN, HXeNC, and HKrCN in Kr and Xe, J. Chem. Phys. 109 (1998) 618–625.
[72] D.C. Cowles, M.J. Travers, J.L. Frueh, G.B. Ellison, Photoelectron spectroscopy of CH_2N^-, J. Chem. Phys. 94 (1991) 3517–3528.
[73] M. McCluskey, H. Frei, Transfer of CH_2 from Ketene to NO by photoexcitation of reactant pairs in solid argon below the CH_2═C═O dissociation limit, J. Phys. Chem. 97 (1993) 5204–5207.
[74] Y.X. Yu, S.M. Li, Z.F. Xu, Z.S. Li, C.C. Sun, An ab initio study on the reaction NH_2 + CH_4 → NH_3 + CH_3, Chem. Phys. Lett. 296 (1998) 131–136.
[75] B. Jing, J.Y. Liu, Z.S. Li, Y. Wang, L. Wang, H.Q. He, C.C. Sun, Direct dynamics studies on the hydrogen abstraction reactions CF_3O + $CH_4(CD_4)$ → $CF_3OH(CF_3OD)$ + $CH_3(CD_3)$, J. Mol. Struct. (THEOCHEM) 732 (2005) 225–231.
[76] F. Mao, R.B. Barat, Minimization of NO during staged combustion of CH_3NH_2, Combust. Flame 105 (1996) 557–568.
[77] G.S. Hammond, A correlation of reaction rates, J. Am. Chem. Soc. 77 (1955) 334–338.